375-395nm UV Generation in Zn-indiffused MgO-doped PPLN Waveguides pumped by an Alexandrite Laser

GORONWY TAWY,[1,*] NOELIA PALOMAR DAVIDSON,[1], REX H. BANNERMAN,[1] GLENN CHURCHILL,[1] PETER G. R. SMITH,[1] JAMES C. GATES[1] AND CORIN B. E. GAWITH[1,2]

[1] *Optoelectronics Research Centre, University of Southampton, Southampton, Hampshire SO17 1BJ, UK*
[2] *Covesion Ltd, Unit F3, Adanac North, Adanac Drive, Nursling, Southampton, SO16 0BT, UK*
[*] *g.l.tawy@soton.ac.uk*

Abstract: We present results of wide wavelength coverage in the ultra-violet (UV) from a Zn-indiffused MgO-doped periodically-poled lithium-niobate (PPLN) waveguide. A continuous tuning range of 375-395 nm is obtained via second-harmonic-generation (SHG) in $\Lambda = 6.1 - 6.9\,\mu$m poled gratings using a single continuously tunable Alexandrite pump laser. Detailed results of the waveguide modes are provided and are shown to match well with the theoretical model. A maximum UV power of 4.1 mW is obtained from 200 mW of throughput pump power from the third-order SHG interaction, providing a route towards a compact and rugged laser source across the 350-400 nm UV range.

1. Introduction

Laser sources emitting in the ultra-violet (UV) are of increasing importance for applications in quantum technologies such as photon pair generation in the near-infrared [1] and atom trapping [2]. Laser diodes offer compactness and simplicity but lack spectral versatility, with commercially available UV sources only being available at 375 nm. Frequency-shifted Nd-doped, Yb-doped and Er-doped solid-state lasers offer a good alternative with high-brightness, compactness and power scalability [3]. However, they lack spectral versatility in the UV range with two or more frequency conversion stages required and typically selective rather than tunable wavelength coverage.

An alternative solution is to use diode-pumped Alexandrite lasers as the pump source with a single stage conversion to the UV. Alexandrite lasers have emerged over the last decade as a highly versatile laser source in continuous wave [4, 5], Q-switched [6] and mode-locked operation [7] with good wavelength versatility at around 700-800 nm enabling access to the UVA range via second-harmonic-generation (SHG) [7]. An additional advantage of Alexandrite compared to other near-infrared lasers (e.g. Cr:LiSAF, Ti:Sapphire) is its low-threshold (<50 mW possible [8]) and its ability to operate at elevated temperatures [9].

High efficiency SHG conversion from Alexandrite lasers can be obtained using bulk nonlinear crystals such as BBO or LBO in a single-pass scheme using a high-energy Q-switched pulse [6] or in an internal Q-switched cavity [10]. However, owing to the low gain of Alexandrite, high-power diode pumping (typically >5 W) is required to achieve laser threshold in these systems. Implementing a system into an environment with small size, low-power and air-cooling requirements therefore requires an alternative solution.

Quasi-phase matched integrated nonlinear optical materials are a growing area of interest for SHG applications. For example, thin-film lithium niobate (TFLN) is an effective way of achieving high efficiency conversion (typically >1000%/W) and has recently shown wide wavelength versatility in the UV with 355-386 nm demonstrated by Hwang et al. [11]. However, its low power-handling (typically <100 µW) prevents its implementation into the aforementioned applications which typically require milliwatts of power.

Periodically-poled QPM ridge waveguides (such as PPLN, PPKTP and PPLT) have lower efficiencies compared to TFLN but have been shown to handle watt-level of optical power. For example, 2.5 W has been achieved with 70 % conversion efficiency for 780 nm generation using Zn-indiffused MgO-doped PPLN waveguides [12]. Compared to other materials, the superior nonlinear coefficient and commercial availability of LN make it a suitable platform for accessing the UVA range.

Building on our previous work where we demonstrated the novel feature of a temperature tunable UV laser based on an Alexandrite laser and PPLN waveguides [9], in this work we share a broader set of results showing wider wavelength versatility, study of the waveguides modes with comparison to detailed theoretical modelling, and the power scalability.

2. Tunable Alexandrite Pump Laser

The Alexandrite laser used in this work was designed for flexibility in power and with wavelength tuning to address the SHG range of the $\Lambda = 6.1 - 6.9\,\mu$m poled waveguides. Figure 1 shows a schematic of the laser cavity.

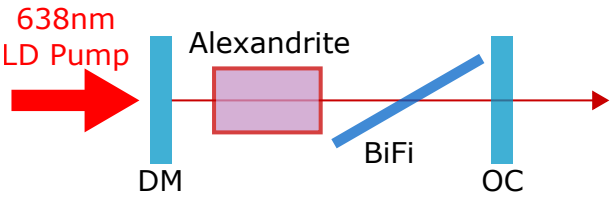

Fig. 1. Schematic diagram of the laser diode pumped Alexandrite laser cavity.

Laser-pumping is provided by a 10 W fibre-coupled red laser diode (BWT Beijing). The output of the 200 µm fibre is imaged onto the crystal to a spot size of around $w_p = 215\,\mu$m. The crystal has a 4×4 mm cross section and is 6 mm long with 0.2 at.% Cr-doping. The laser diode output has a mixed polarisation with around 80 % of the incident pump power absorbed by the crystal.

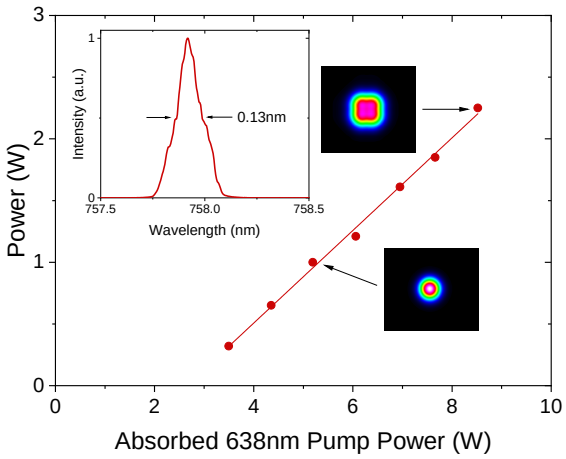

Fig. 2. Alexandrite laser power as a function of absorbed 638 nm power. Inset: Beam profile at different powers and laser spectrum at 5.2 W absorbed power.

The plane-plane cavity is formed of a dichroic mirror (DM) which is highly transmissive (HT) at the laser diode pump wavelength and highly reflective (HR) at the laser wavelength, and an output coupler (OC) with a reflectivity of 99 % at the laser wavelength. A 1 mm birefringent

filter (BiFi) is used to tune the laser wavelength. Its free spectral range of ~ 60 nm [5] does not cover the full-bandwidth of Alexandrite but does cover the SHG range of the waveguides used in this work. The laser output is later coupled into a 780 nm polarisation-maintaining fibre delivered to the waveguide setup.

A maximum output power of 2.25 W is obtained at an absorbed pump power of 8.52 W with an overall slope efficiency of 38 %, as shown in Fig. 2. For optimal launching into the polarisation-maintaining fibre the laser is operated at an absorbed pump power of 5.2 W where the Alexandrite laser power is 1 W (at 757.9 nm) and the beam quality M^2 = 1.2. Improved beam quality at higher-power can be easily achieved using a modified laser cavity design [5], but the power here is more than sufficient for testing the waveguides. Figure 3 shows the Alexandrite laser power as a function of the wavelength achieved via rotation of the intracavity birefringent filter. A continuous tuning range of 734-790 nm was obtained with a laser linewidth of <0.15 nm.

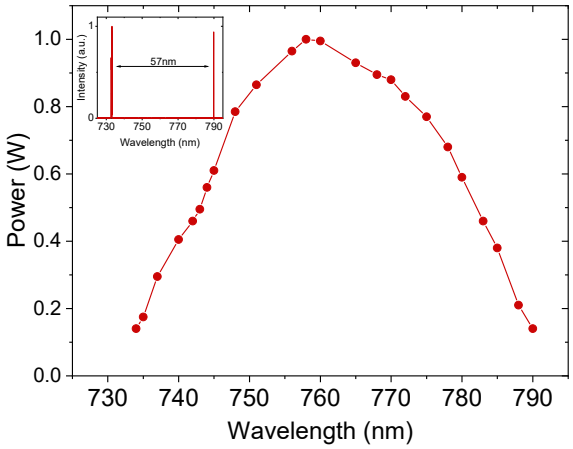

Fig. 3. Alexandrite laser power at 5.2 W absorbed power (638 nm) as a function of wavelength. Inset: Dual wavelength operation due to free spectral range of 1 mm BiFi.

3. Zn-indiffused MgO-doped PPLN Waveguides

3.1. Properties and Setup

We have adopted planar Zn indiffusion to form the vertical confinement and high-precision dicing for horizontal confinement in MgO-doped PPLN wafers. Figure 4 shows the fabrication steps, starting with 5 % MgO-doped PPLN wafers (0.5 mm thick), a thin-film deposition of ZnO is applied and then indiffused in an oxygen-rich environment. This is followed by ductile dicing to form chips with multiple waveguides. Further details of the waveguide fabrication can be found in our previous work [13]. With control of the Zn thickness, indiffusion temperature and waveguide width, this technique has proven to be a reliable and repeatable method for fabricating 1560 nm to 780 nm SHG waveguides with high device efficiency and low-loss [12].

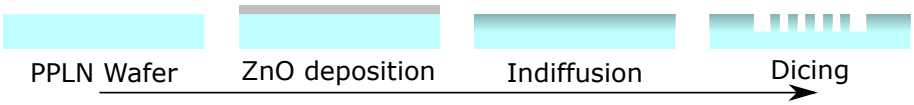

Fig. 4. Fabrication steps for our Zn-indiffused Mgo-doped PPLN waveguides.

PPLN wafers with poling periods Λ = 6.1, 6.3, 6.5, 6.7 and 6.9 µm were used. Designed

for SHG at 1064 nm, they also work for third-order SHG at around 780 nm and so can give a good indication of performance without requiring fabrication of ~ 2 µm first-order periods. For supporting modes at visible (532 nm) wavelengths, the waveguide design is adapted by reducing the Zn layer thickness to 47 nm and lowering the indiffusion temperature to 900 °C [14]. Nominal waveguides widths of 5-7 µm in 0.5 µm steps are diced into 10 mm and 20 mm long chips with a 5.3° angle cut to minimise back reflections.

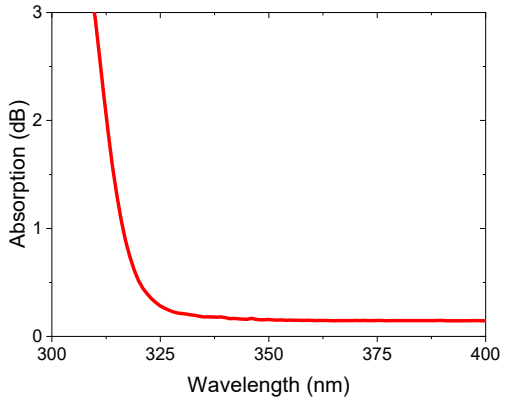

Fig. 5. Absorption loss as a function of wavelength over the UVA region.

To asses the viability of operation in the ultra-violet (UV), a spectrophotometer measurement was performed to measure the absorption profile of a MgO-doped wafer. Figure 5 shows the absorption over the UVA-region with a significant increase at <325 nm indicating that operating above this wavelength should be possible without any significant absorption losses.

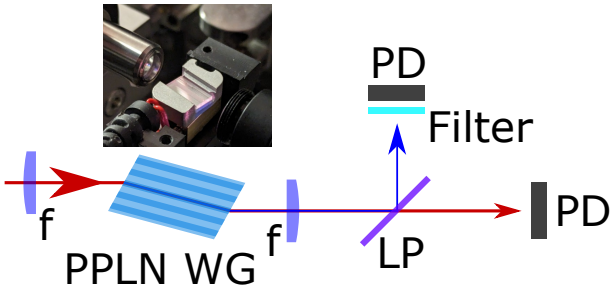

Fig. 6. Schematic diagram of the waveguide SHG setup, and photo of the PPLN chip containing the waveguides.

The waveguide phase-matching and efficiency characteristics were analysed by using the setup shown in Fig. 6. The fibre-coupled output of the Alexandrite pump laser is collimated using a zoom-collimator and focused into the waveguide using a f = 11 mm aspheric lens to a spot size of around 2-3 µm. The pump laser throughput and UV signal are collimated by a secondary f = 11 mm aspheric lens then split using a longpass dichroic mirror (LP) onto separate photo-diodes (PD) for power measurements. An additional filter is used to prevent any unwanted measurement of the pump laser. A 0.02 nm resolution optical spectrum analyser and scanning beam profiler are also used to measure the laser spectra, and transverse mode profile. This setup allows testing of the SHG performance for both the 10 mm and 20 mm long waveguides in chips which are mounted onto a Covesion P20 oven for temperature control at 20-200 °C.

3.2. *Phase-Matching*

To analyse the broad phase-matching performance, chips of each poling-period were used in the setup with the pump laser wavelength fixed and the temperature of the waveguide varied over the full 20-200 °C range. The incident laser power was set to around 100 mW. 10 mm-long chips were used to analyse the first four poling-periods ($\Lambda = 6.1 - 6.7\,\mu m$) and a 20 mm-long chip for the final $\Lambda = 6.9\,\mu m$ poling-period.

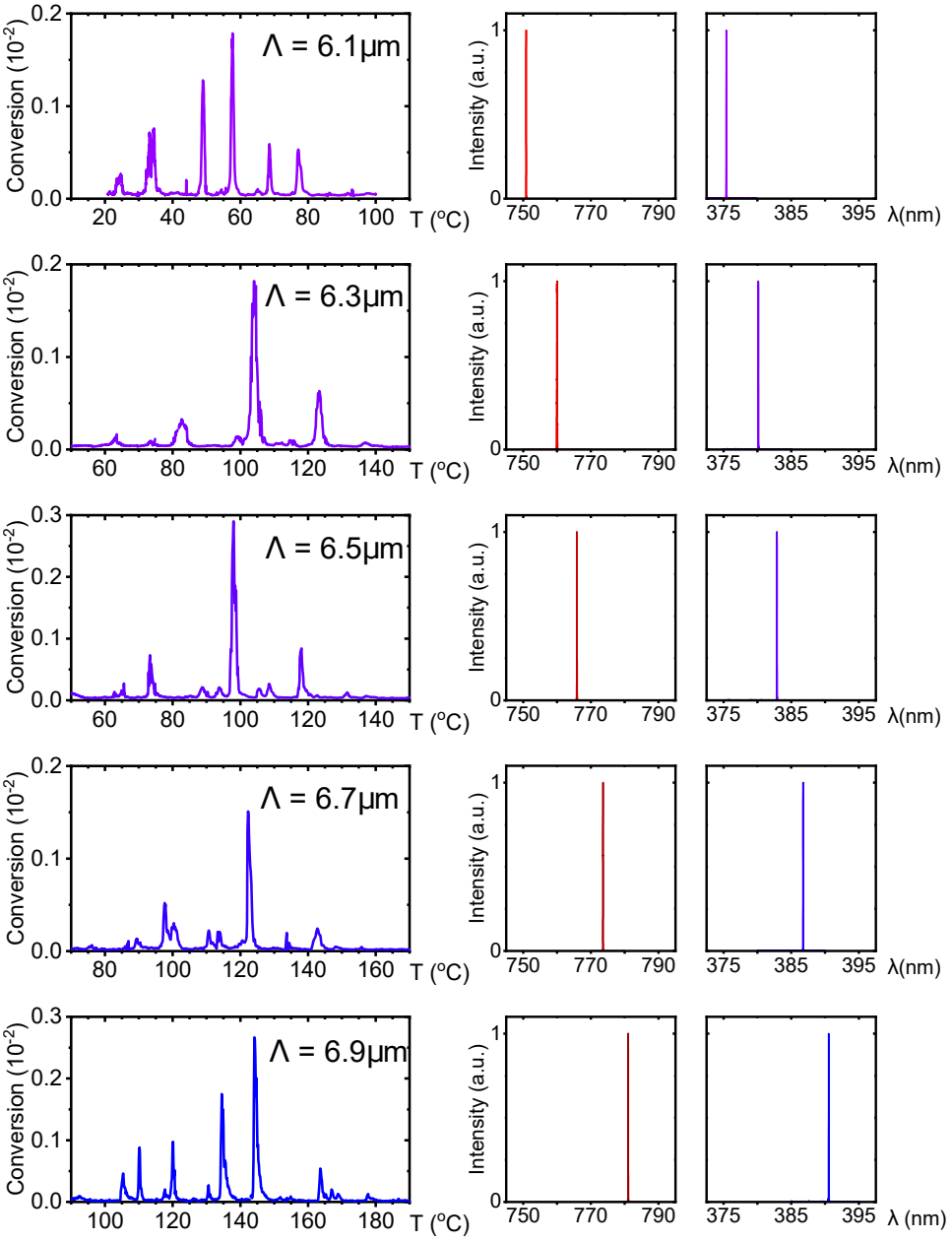

Fig. 7. Overview of phase matching results for all five poled waveguides. Results show conversion measured as a function of PPLN temperature at 750, 760, 766, 773 and 781 nm. Laser infrared pump and UV signal spectra are also shown.

Figure 7 shows the conversion (UV power divided by laser pump power) for the 7.0 µm wide waveguide in each of the five prepared chips, with the pump and signal spectrum for each measurement also shown. Phase matching was achieved in each of the five waveguides with multiple UV signal peaks observed over a 60 °C temperature range. The same peaks were observed for each poling-period with slight variation in the relative intensities. Wavelength tuning across a single waveguide was achieved by varying the temperature. For example, Fig. 8 shows the phase matching data for the $\Lambda = 6.1$ µm poled waveguide (7.0 µm waveguide width) at pump wavelengths of 750.9 nm and 760.0 nm, showing that a UV tuning range of around 375-380 nm can be achieved for this waveguide - though the full tuning range is 373.7-381.9 nm when including just a single phase matching peak. A total UV tuning range of 373.7-393.6 nm was obtained across all $\Lambda = 6.1 - 6.9$ µm waveguides.

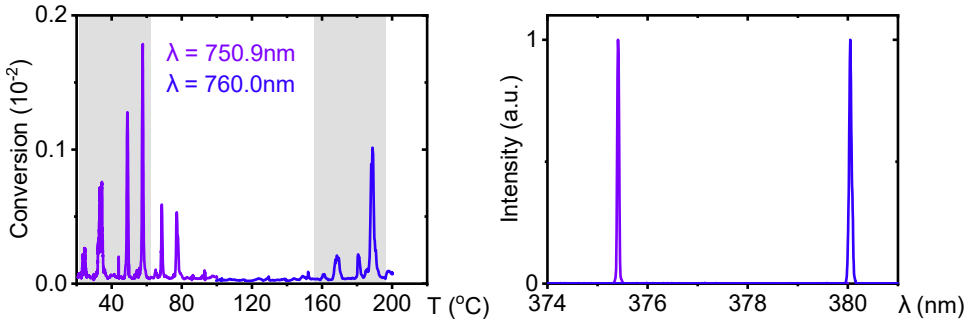

Fig. 8. Conversion for $\Lambda = 6.1$ µm poled waveguide (7.0 µm waveguide width) at two fixed wavelengths of 750.9 nm and 760.0 nm and the generated UV spectrum. Grey-region indicates the repeated peaks - the reduction in efficiency is attributed to a broader bandwidth at 760.0 nm.

3.3. Waveguide Modes

To further study the phase matching peaks, and to compare different waveguide widths, the laser pump wavelength was fixed to 776.2 nm (incident pump power of 215 mW) and coupled into the 5.0 and 7.0 µm-wide waveguides in the $\Lambda = 6.7$ µm chip. The output power of the UV signal and infrared throughput pump were measured (as shown in Fig. 6) as well as the mode profile of the UV signal.

Figure 9 shows the phase matching results of two $\Lambda = 6.7$ µm chips with the mode profile (far-field) of the UV signal. The 7.0 µm wide and 10 mm long waveguide (top left in Fig. 9) has six clear peaks corresponding to six different transverse magnetic modes with high efficiency for the TM_{11} and TM_{01} modes. The TM_{00} is present but has low efficiency. The large number of modes found here is due to the 7.0 µm-wide waveguide being primarily designed for SHG at 1064 nm and therefore the waveguide width and refractive index diffusion parameters are suited to a larger mode size at both the fundamental and second harmonic. This therefore allows phase matching of the TM_{00} and higher-order pump modes to a range of UV modes.

To verify this, a model of the waveguide was built using the FIMMWAVE software. Figure 10 shows the parameters of the waveguide where the refractive index is assumed to have a Gaussian profile in the vertical direction of the form $n = n_{sub} + \Delta n e^{-(y/\sigma)^2}$ where n_{sub} is the refractive index of the lithium niobate substrate, Δn is the maximum refractive index change and σ is the diffusion depth. These parameters are determined by comparing a planar layer of the model to values measured using a Metricon prism coupler. The FIMMWAVE model provides solutions for all the possible modes of the waveguide at both the pump and signal wavelengths.

To compare the model with the results, the temperature dependence of the effective index of

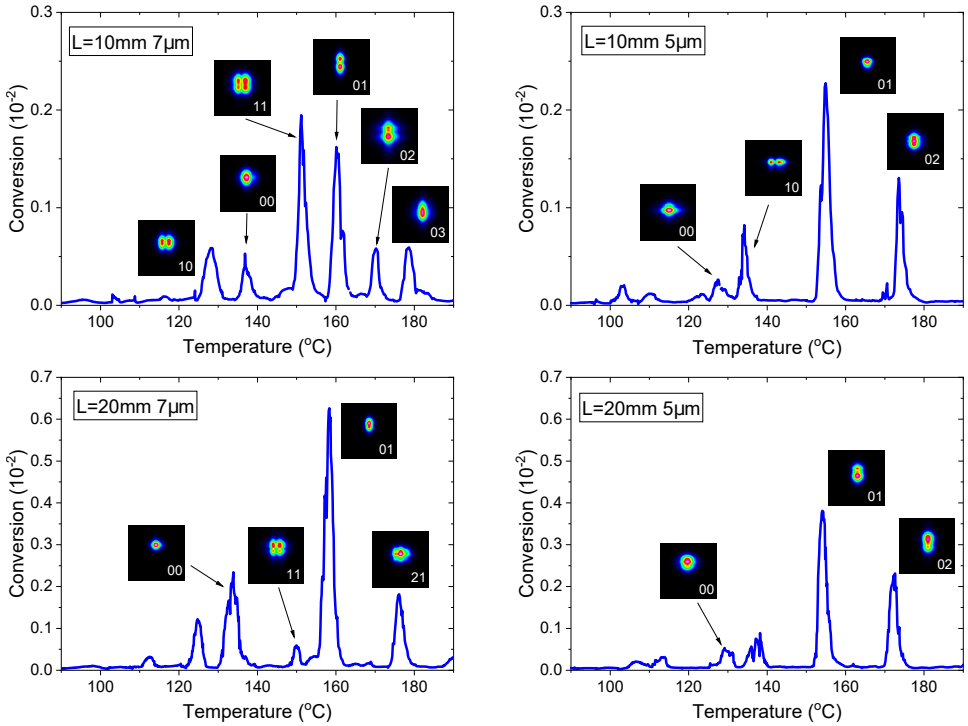

Fig. 9. Phase matching results for four $\Lambda = 6.7$ µm waveguides with a fixed pump laser wavelength of 776.2 nm.

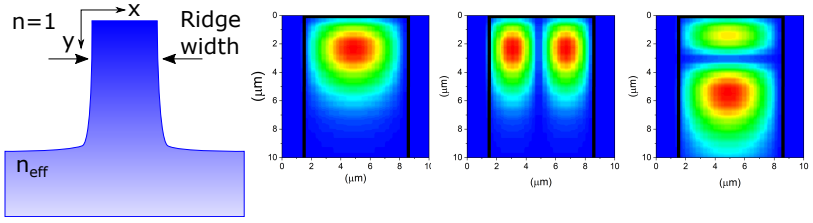

Fig. 10. Waveguide model and examples of the transverse mode profiles of the pump in the 7.0 µm-wide waveguide.

the waveguide modes at both the pump and signal wavelengths were calculated. Figure 11 shows the possible phase matching conditions for six of the waveguide modes with the lowest-loss and highest overlap in the 7.0 µm-wide waveguide, and a comparison to the experimental results. The model matches the experiment reasonably well, indicating that the UV modes observed are from both the TM_{00} and TM_{10} pump modes. The temperature offset can be attributed to the error in the real and calculated values of σ and Δn, though the temperature separation between the peaks is in reasonable agreement. The model did not show a major difference in the conversion efficiency between the different modes, which was found in the experiment. This may be due to irregularity in the ridge width which was not included in the model.

Figure 12 shows a comparison of the FIMMWAVE model to the experimental results in the 5.0 µm waveguide. In this waveguide, there are no higher-order modes expected at the pump wavelength, and therefore the TM_{11} mode is lost and the TM_{00} mode is the lowest temperature mode. Again, the highest measured efficiency is obtained in the higher-order TM_{01} mode. The

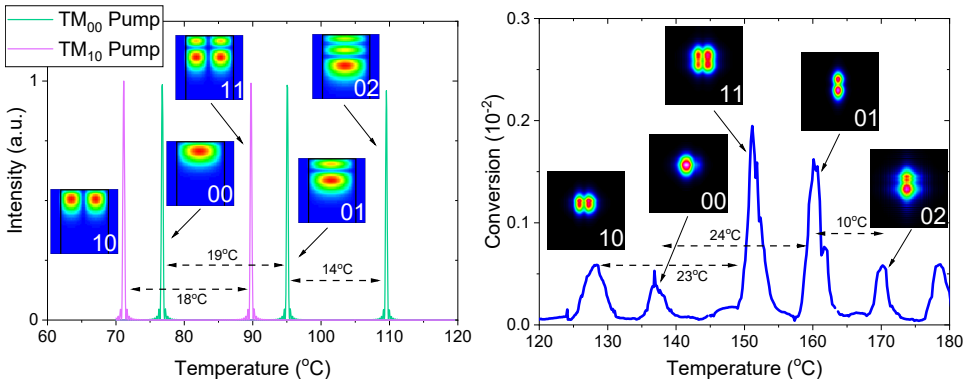

Fig. 11. Phase matching results for the $\Lambda = 6.7\,\mu$m waveguide ($L = 10$ mm, 7.0 µm-wide) with a fixed pump laser wavelength of 776.2 nm. Left figure shows FIMMWAVE model, and right figure shows experimental result.

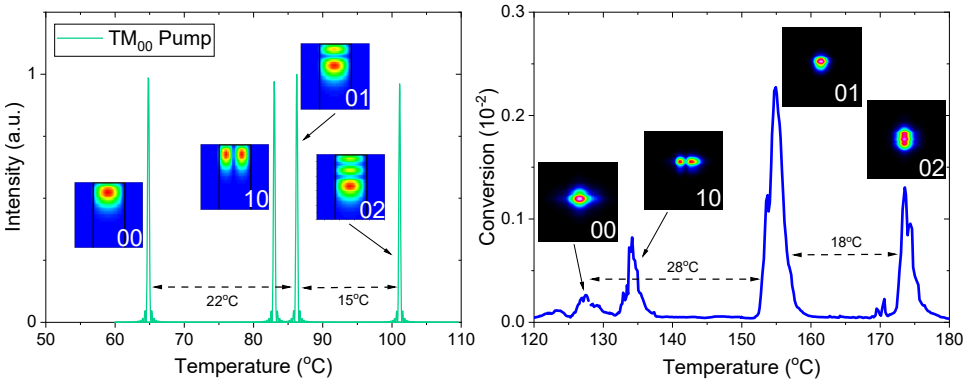

Fig. 12. Phase matching results for the $\Lambda = 6.7\,\mu$m waveguide ($L = 10$ mm, 5.0 µm-wide) with a fixed pump laser wavelength of 776.2 nm. Left figure shows FIMMWAVE model, and right figure shows experimental result.

TM_{00} mode efficiency is again low as the refractive index diffusion is the same as for the 7.0 µm wide waveguide.

When comparing the experimental results of the 10 mm and 20 mm-long waveguides (Fig. 9) there are slight changes. In the 7.0 µm-wide waveguide, the efficiency of the TM_{11} has fallen, the TM_{02} and TM_{03} are lost and another higher-order mode is found. This is likely due the variation in the ride-width and refractive index diffusion over a longer length causing loss to higher-order modes. This is also found in the 5.0 µm-wide waveguide where the TM_{10} mode efficiency has reduced.

While some applications require single-mode operation there is growing interest in developing laser sources operating in higher-order modes [15] as a platform for generating complex beams in material processing [16]. Our system provides a simple and versatile platform for achieving high-order UV modes. For higher efficiency single-mode operation in the UV range, the waveguide parameters can be adapted to a narrower waveguide and shallower indiffusion profile. We have recently demonstrated initial results of a waveguide design model that covers the entire transparency range of PPLN [14] and are in progress of publishing the full results.

3.4. Power

Figure 13 shows the signal power as a function of the throughput pump power in the low-depletion region. This initial measurement is made at a pump laser wavelength of 774.4 nm phase matched to the TM_{01} mode in the $\Lambda = 6.7\,\mu m$ ($L = 10$ mm, 7.0 µm-wide) waveguide. The phase matching spectrum is also shown indicating a 0.7 °C temperature bandwidth - theoretical value is around 1.0 °C. Figure 13 also shows the green power obtained for first-order SHG at 1063.0 nm (using a Nd:$GdVO_4$ laser) and its phase matching spectrum.

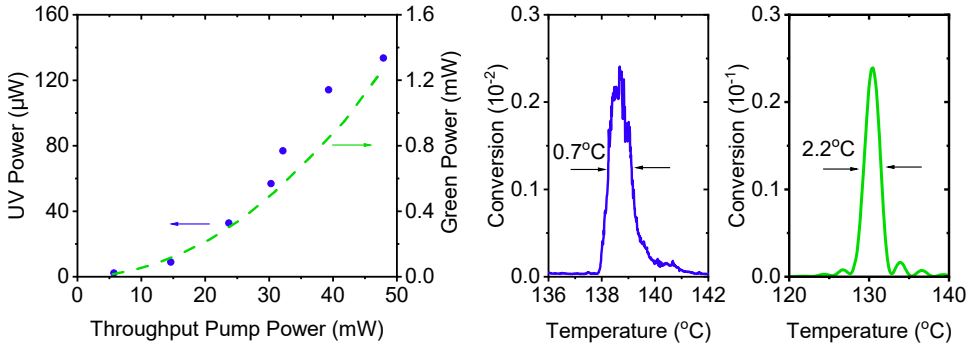

Fig. 13. UV and green power as a function of throughput pump power in the low-depletion region and the corresponding temperature phase matching curves.

The results show a quadratic increase in power and that the UV signal power generated is around a tenth of that for the first-order 1063.0 nm to 531.5 nm conversion, as expected [17]. The loss (including coupling, absorption and Fresnel from the uncoated surfaces) is calculated by comparing the incident and throughput pump laser power and found to be 5.2 dB cm^{-1} and 4.3 dB cm^{-1} at 774.4 nm and 1063.0 nm, respectively. To asses higher power operation, the pump power was increased and the 20 mm-long waveguide was also used. Figure 14 shows the UV signal power as a function of the throughput pump power for both 10 mm and 20 mm long waveguides.

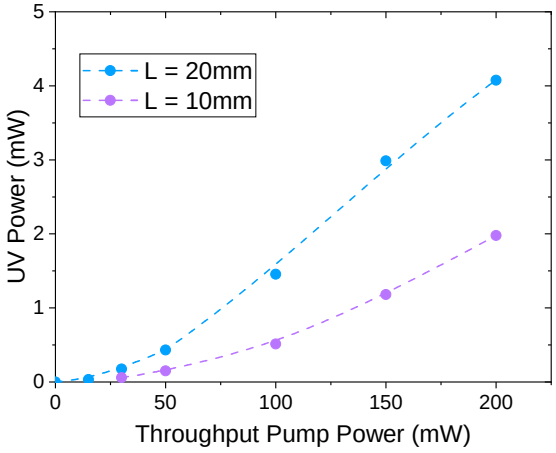

Fig. 14. UV power (at 387.2 nm) as a function of throughput pump power for $\Lambda = 6.7\,\mu m$ 10 mm and 20 mm long waveguides.

A maximum UV power of 4.1 mW is obtained at a throughput pump power of 200 mW using

the 20 mm waveguide, corresponding to conversion efficiency of 2 %. The signal power is however limited by the linewidth of the pump laser. Based off the phase matching results, the refractive index difference is $\Delta n = 0.1734$ at 774.4 nm, giving a pump laser linewidth bandwidth of around $\Delta\lambda = 0.08$ nm for the $L = 20$ mm long waveguide - less than the 0.15 nm linewidth of the Alexandrite laser. With a <0.08 nm linewidth, then based off the power levels obtained from the 10 mm waveguide, first-order $\Lambda = 2.0 - 2.5$ µm poling-periods would theoretically enable an efficiency of >25 % and 50-100 mW of UV power from a 20 mm waveguide.

4. Conclusion

We have shown that Zn-indiffused MgO-doped PPLN waveguides offer a suitable platform for achieving laser operation across the UVA range, with 373.7-393.6 nm continuous wavelength tuning achieved using third-order second-harmonic-generation (SHG) in $\Lambda = 6.1 - 6.9$ µm poled ridge waveguides. A comprehensive analysis and modelling of the waveguide modes has been provided, indicating the additional modal flexibility of this system.

Using an Alexandrite laser pump, 4.1 mW of UV poower is obtained from 200 mW throughput power. Optimisation in the pump laser linewidth, anti-reflection coatings of the waveguides for reducing loss, and a dedicated design of the waveguide for UV operation with first-order poling, and improved Zn-indiffusion will enhance the performance of this system. Having demonstrated over 100 mW of green with 40 % conversion efficiency using these waveguide [14], optimisation of this platform provides a route to similar levels of UV from a single-emitter multimode red laser diode. Broader spectral coverage from a single waveguide can be achieved using a fan grating, giving great potential for a highly versatile compact and rugged UV laser source.

Funding

Engineering and Physical Sciences Research Council (EP/P027644/1, EP/T00097X/1); Royal Academy of Engineering (RCSRF1718639); Innovate UK (10001664, 50414).

Disclosures

PGRS and CBEG: Covesion Ltd. (E,P). All other authors declare no conflicts of interest.

References

1. B. Li, Y.-H. Li, Y. Cao, *et al.*, "Pure-state photon-pair source with a long coherence time for large-scale quantum information processing," Phys. Rev. Appl. **19**, 064083 (2023).
2. J. MacArthur, S. P. Najda, A. E. Kelly, *et al.*, "Compact GaN based sources for atomic cooling," in *Quantum Sensing, Imaging, and Precision Metrology II,* vol. PC12912 J. Scheuer and S. M. Shahriar, eds., International Society for Optics and Photonics (SPIE, 2024), p. PC1291238.
3. D. Li, C.-Y. Huang, X.-W. Chang, *et al.*, "Continuous-wave self-raman vanadate lasers generating versatile visible wavelengths," Photonics **11** (2024).
4. G. Tawy, A. Minassian, and M. J. Damzen, "Volume bragg grating locked alexandrite laser," Optics **3**, 53–59 (2022).
5. G. Tawy, A. Minassian, and M. J. Damzen, "Power-scaled cw alexandrite lasers," Appl. Phys. B **129**, 47 (2023).
6. M. Liang, A. Minassian, and M. J. Damzen, "High-energy acousto-optic q-switched alexandrite laser with wavelength tunable fundamental and uv second harmonic generation," Opt. Express **31**, 42428–42438 (2023).
7. C. Wang, J. B. Khurgin, and H. Yu, "589nm yellow laser pumped kerr-lens mode-locked alexandrite laser producing sub-50fs pulses," Opt. Lett. **48**, 6248–6250 (2023).
8. I. Yorulmaz, E. Beyatli, A. Kurt, *et al.*, "Efficient and low-threshold Alexandrite laser pumped by a single-mode diode," Opt. Mater. Express **4**, 776–789 (2014).
9. G. Tawy, N. P. Davidson, G. Churchill, *et al.*, "Temperature-tunable uv generation using an alexandrite laser and ppln waveguides," Opt. Express **31**, 22757–22765 (2023).
10. S. Scheuer, A. Munk, M. Strotkamp, *et al.*, "Efficient intra-cavity frequency doubled, diode-pumped, q-switched alexandrite laser directly emitting in the uv," Opt. Express **32**, 7553–7563 (2024).
11. E. Hwang, N. Harper, R. Sekine, *et al.*, "Tunable and efficient ultraviolet generation with periodically poled lithium niobate," Opt. Lett. **48**, 3917–3920 (2023).
12. L. G. Carpenter, S. A. Berry, A. C. Gray, *et al.*, "CW demonstration of SHG spectral narrowing in a PPLN waveguide generating 2.5 W at 780nm," Opt. Express **28**, 21382–21390 (2020).

13. L. G. Carpenter, S. A. Berry, R. H. S. Bannerman, *et al.*, "ZnO indiffused MgO:PPLN ridge waveguides," Opt. Express **27**, 24538–24544 (2019).
14. N. P. Davidson, G. Tawy, G. M. Churchill, *et al.*, "Developing zinc-indiffused PPLN ridge waveguides for UV, visible and MIR quantum applications," in *Nonlinear Frequency Generation and Conversion: Materials and Devices XXIII,* vol. PC12869 P. G. Schunemann, ed., International Society for Optics and Photonics (SPIE, 2024), p. PC128690A.
15. J. W. T. Geberbauer, W. R. Kerridge-Johns, and M. J. Damzen, ">30 W vortex LG01 or HG10 laser using a mode transforming output coupler," Opt. Express **29**, 29082–29094 (2021).
16. A. Tomita, A. Vallés, K. Miyamoto, and T. Omatsu, "Creation of galaxy-shaped vortex relief structures in azo-polymers with petal-like beams," Opt. Express **31**, 27868–27879 (2023).
17. W. P. Risk, T. R. Gosnell, and A. V. Nurmikko, *Compact Blue-Green Lasers* (Cambridge University, 2003).